Signature of Proton–Hole Transfer in Hydrogen-Bonded Solids at 10 K

Kensei Kitajima[†], *Yoichi Nakai*[†,‡], *Masashi Tsuge*[†], *Naoki Watanabe*[*,†]

[†] Institute of Low Temperature Science, Hokkaido University, Sapporo 060-0819, Japan

[‡] RIKEN Nishina Center for Accelerator-based Science, Wako 351-0198, Japan

Corresponding Author

*E-mail: watanabe@lowtem.hokudai.ac.jp

ABSTRACT. Although proton transport in water ice is well understood, proton–hole transfer (PHT) involving proton abstraction by anions remains less explored. This study investigates PHT in H_2S and NH_3 solids at low temperatures, aiming to determine if these solids exhibit negative charge transport similar to that in ice. In H_2S and NH_3 solids at 10 K, surface HS^- and NH_2^- anions in hydrogen-bonded systems trigger negative current flow, providing a clear signature of PHT. This negative current is controlled by electron flow and 193 nm ultraviolet irradiation, which generates HS^- and NH_2^- anions on the solid surfaces. In bilayer H_2S/H_2O and NH_3/H_2O solids, a significant negative current is observed only in the NH_3/H_2O solid, which is attributed to the exothermic proton abstraction reaction of NH_2^- with H_2O at the bilayer interface—a process not available for H_2S on ice. This study is the first to demonstrate PHT-induced electrochemical behavior in hydrogen-bonded solids other than ice.

TOC GRAPHICS

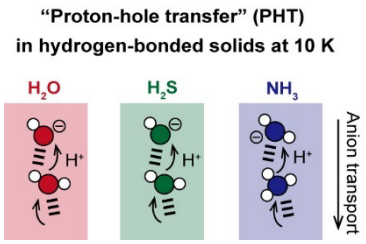

KEYWORDS. Solid hydrogen sulfide, Solid ammonia, Hydrogen bond, Proton–hole transfer, Ultraviolet photons, Electrons.

Proton transport through hydrogen bonds plays a crucial important role in environments related to acid/base chemistry, biochemistry, and atmospheric chemistry[1–5]. Water ice has long been studied to understand proton transfer through chains of hydrogen bonds. The unique electrochemical property of water ice, resembling a 'p-type semiconductor,' has been characterized by the Grotthuss mechanism[1,6], which demonstrates that excess protons are relayed along hydrogen bonds. Many experimental and theoretical studies have attempted to clarify the conductivity of protons in ice. These studies suggested that protons exhibit anomalous physicochemical behavior even at low temperatures[7–11]. However, while the proton transfer mechanism in ice is well understood, knowledge about proton–hole transfer (PHT), involving proton abstraction by anions such as OH^- remains limited. In recent years, negative charge transport in ice at temperatures below 50 K, which is governed by PHT, has been demonstrated[12,13]. This phenomenon is observed when ice is simultaneously exposed to ultraviolet (UV) photons and electrons. The negative charge transport was confirmed by measuring the negative current at the metal substrate under ice. We suggested a scenario in which UV-photodissociated OH from H_2O captures an electron on ice and trigger PHT, $OH^- + H_2O \rightarrow H_2O + OH^-$, which continues until OH^- reaches the metal substrate under ice. Quantum chemical calculations for the PHT pathway in ice indicated that potential energies of ice-metal system including OH^- anion in ice decrease gradually from vacuum-ice to ice-metal boundaries[13]. Based on the temperature independence and non-isotope effect observed during this phenomenon, PHT is believed to be barrierless or have a low barrier in ice, as confirmed by quantum chemical calculations[12]. However, this feature contrasts with the Grotthuss mechanism, which postulates that such processes possess moderate activation barriers[14,15]. Therefore, in this

study, we propose that solids with hydrogen-bonded networks, other than ice, may also exhibit negative charge transport via the PHT mechanism at low temperatures.

H_2S and NH_3 are typical molecules that form hydrogen bonds through intermolecular interactions in solids[16]. For example, neutron powder diffraction measurements have demonstrated that H_2S and NH_3 solids form hydrogen-bonded crystal structures at low temperatures[17,18]. The infrared spectra of amorphous H_2S and NH_3 solids exhibit multiple absorption peaks in the hydrogen stretching region, suggesting the existence of a hydrogen-bond network[19–21]. For cation/anion dimer systems of H_2S and NH_3, previous studies have explored proton transfer reactions along hydrogen bonds, revealing a symmetric potential energy profile in the system[22–26]. Nevertheless, the negative charge transport in hydrogen-bonded molecular solids, other than ice, and its mechanisms have not been elucidated[12,13]. To gain comprehensive understanding of PHT, it is important to examine the PHT-induced negative current in hydrogen-bonded molecular solids, such as H_2S and NH_3, in addition to ice. Therefore, in this study, we observed negative charge delivery in H_2S and NH_3 solids at 10 K, which is the signature of PHT occurring in hydrogen-bonded systems. For H_2S solids, the behavior of surface HS radicals upon electron exposure was investigated. In addition, the currents transmitted through bilayer solids (i.e., H_2S/H_2O and NH_3/H_2O) were measured.

In analogy with the PHT process in ice, HS^- and NH_2^- are considered to initiate PHT in H_2S and NH_3 solids, respectively. In this study, the H_2S and NH_3 solids in amorphous phase with the thickness of ~80 monolayers were produced by vapor deposition at 10 K over a nickel (Ni) substrate plated on a sapphire disk. The current through the solids was measured at the Ni substrate of which the surface would be oxidized to some extent in air. HS and NH_2 radicals were produced by 193 nm UV irradiation. Electrons were supplied from an electron-gun to the surface to form

HS^- and NH_2^- to initiate PHT; see Supporting Information for the details of experimental methodology. In the photochemical reaction of H_2S solids upon 193 nm UV irradiation, HS was the primary product, with additional species such as S forming when HS undergoes further photolysis[27,28]. The dissociation cross section of HS was $\sim 5\times10^{-18}$ cm^2, which was comparable to that of H_2S at 193 nm[29]. Therefore, a certain amount of S atoms would exist on the surface. However, because proton abstraction by S^- anions from H_2S was endothermic according to the gas-phase proton affinity[30], they cannot work for PHT. Thus, HS^- most likely becomes the trigger for PHT in H_2S solids. In the 193 nm UV photolysis of NH_3 solids, NH_2 was the main product, which may recombine to form N_2H_4[31–33] or absorb additional photons to produce NH and H[31–33]. However, the dissociation cross section of NH_2 was $\sim 10^{-21}$ cm^2, which was four orders of magnitude smaller than that of NH_3 (10^{-17} cm^2) at 193 nm[29]. Thus, the contribution of NH to initiate PHT was negligible. Therefore, the main dissociation products that triggered PHT should be HS for H_2S and NH_2 for NH_3. Bulk water exhibits negligible photoabsorption at 193 nm[29], inhibiting the photodissociation of H_2O.

In the experiments with H_2S solids, HS radicals on the surface of solid H_2S were detected by the combination of photostimulated desorption and resonance-enhanced multiphoton ionization (PSD-REMPI) methods[34,35], which have been applied to detect atoms and radicals such as hydrogen atoms[34], hydroxyl radicals[36,37], and carbon atoms[35] on low-temperature solid surfaces. The wavelength of the PSD laser was 532 nm. The photodesorption yields of HS correlated linearly with the PSD laser power, indicating that the photodesorption of HS from an H_2S solid surface was caused by one-photon chemical processes, as previously reported for OH[36]. The details of photodesorption mechanism of H_2S are unclear. Although an isolated HS radical does not absorb photons at 532 nm, the interaction between HS and surrounding H_2S molecules may

induce red-shift of the electronic excitation band leading to desorption of HS radical like the case of OH photodesorption from ice[36].

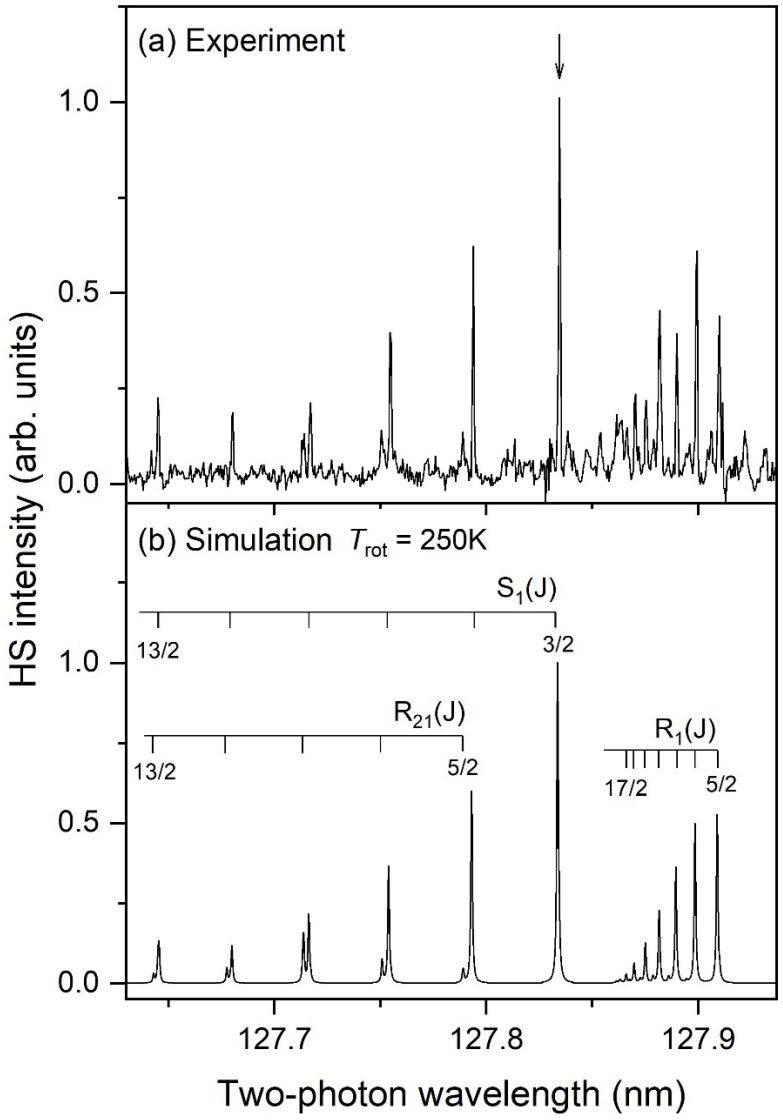

Figure 1. (a) The 2+1 resonance-enhanced multiphoton ionization (REMPI) spectrum of photodesorbed HS radicals. The wavelength of the REMPI laser was set at 255.67 nm for the S_1 (3/2) branch of a transition, $[a^1\Delta]\ 3d\pi\ ^2\Phi\ (v' = 0) \leftarrow X\ ^2\Pi\ (v'' = 0)$, as indicated by an arrow. (b) The simulation result using the PGOPHER program. The individual line assignments are given by the combs above the spectrum.

Figure 1 shows the 2+1 REMPI spectrum of HS radicals photodesorbed by the PSD laser from the H_2S solid surface during 193 nm irradiation. The REMPI laser wavelength was set at 255.67 nm for the S_1 (3/2) branch of transition [$a^1\Delta$] 3dπ $^2\Phi$ ($v' = 0$) ← X $^2\Pi$ ($v'' = 0$). The experimental results agreed with the spectral simulation generated using the PGOPHER program[38], confirming the detection of HS radicals photodeosorbed from the H_2S solid surface. The rotational temperature of desorbed HS was estimated to be 250 K by adapting the rotational constants for HS radicals reported by Milan *et al.*[39]. The calculated rotational temperature was close that for OH radicals (200 K) photodesorbed from ice by a 532 nm photon[13,36].

At low temperatures of ~10 K, the solid surfaces became negatively charged during electron exposure[40,41], causing the incident electrons to decelerate, which prevented H_2S and NH_3 molecule fragmentation by electrons after the solid surface was charged. As shown in Figures 2(a) and 3, the transmission of negative charges in pure solids of H_2S and NH_3 was confirmed upon co-exposure to 193 nm UV photons and electrons. These behaviors were similar to those observed for ice[12,13]. Given that the electron affinities of HS and NH_2 were 2.3 and 0.77 eV, respectively[30], electrons would efficiently attach to radicals to form anions (i.e., HS^- and NH_2^-) on the solid surface. The incident electron currents were controlled below 30 nA cm^{-2} and measured on the nickel substrate before sample gas deposition.

We estimated the production rate of radicals for H_2S and NH_3 solids. Under UV exposure, the photodissociation cross section of H_2S and NH_3 molecules was ~10^{-17} cm^2 at 193 nm[29]. By applying this value, the maximum production rate of the HS or NH_2 radical was estimated to be on the order of 10^{13} cm^{-2} s^{-1}, from the photon flux (f_{uv}) of ~10^{15} cm^{-2} s^{-1} and the surface number density of molecules to be ~10^{15} cm^{-2}. The incident electron currents less than 30 nA cm^{-2} correspond to the electron fluxes less than approximately 10^{11} cm^{-2} s^{-1}, which are well below the

radical production rate. Therefore, the transmitted currents would have been limited by the incident electron densities supplied to the solid surface, assuming that electron attachment to radicals occurred readily.

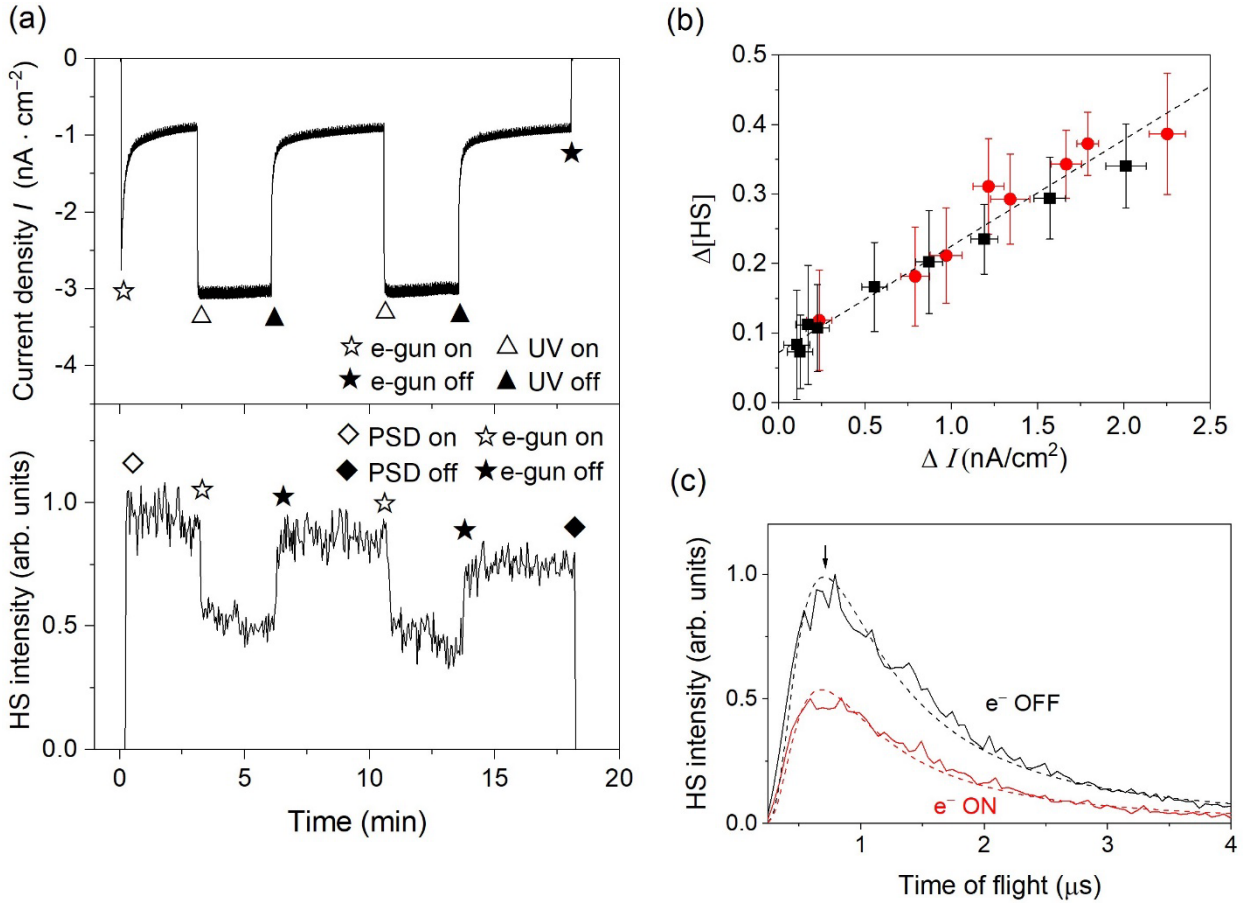

Figure 2. (a) Temporal variation in the negative current density, *I*, during the sequential 193 nm ultraviolet (UV) irradiation of H_2S solids at 10 K with continuous electron gun operation (upper panel). Temporal variation in the HS density, [HS], as monitored by the photostimulated desorption and REMPI (PSD-REMPI) method during the sequential electron exposure of H_2S solids at 10 K upon continuous 193 nm UV irradiation (lower panel). (b) Correlation between the HS radical consumption (Δ[HS]) and increase in the constant negative currents (Δ*I*) in the H_2S solid. The measurement was conducted by increasing the incident electron flux from a lower to

higher incident flux (black squares). By using another H_2S fresh sample, additional data were collected by decreasing the flux from higher to lower (red circles). The dotted line indicates a linear fitting for each data point considering the error bars. (c) Time-of-flight distribution of the desorbed HS radicals for the distance from the solid surface to the focal point of the probe laser with (e^- ON) and without (e^- OFF) electron exposure. Dotted lines refer to the fitting results obtained using the Maxwell–Boltzmann distribution at a translational energy of ~2100 K.

In the Figure 2(a) upper panel, we observe a temporal variation of negative currents in H_2S solids at 10 K upon electron and 193 nm UV exposure. The incident electron flux was ~3 nA cm^{-2}. The sharp transient current peak appears at the electron irradiation onset, and the current immediately decreases due to the solid surface charging. Although the transient current origin is not fully understood, HS radicals formed by electron impact on H_2S solids possibly play a role, as previously reported for ice[13]. That is, because electrons with 30 eV kinetic energy could dissociate H_2S molecules[42,43], HS radicals could be formed at the electron exposure onset and subsequently capture electrons to become HS^- anions as a PHT trigger. After the transient current decreased, a small current was still observed, which is possibly due to different mechanisms such as electron leakage through the surface of pores and cracks and/or grain boundaries or transmission of solvated electrons. Upon 193 nm UV irradiation of the H_2S solid, an additional steady negative current of ~2 nA cm^{-2} appeared immediately and persisted until UV irradiation ceased.

In the Figure 2(a) lower panel, we observe a temporal variation in the surface density of HS radicals detected by PSD-REMPI upon 193 nm UV irradiation. An HS density decrease was observed upon electron exposure. The negative currents increased and the surface HS density decreased simultaneously upon co-exposure of the H_2S solid to 193 nm UV radiation and

electrons, indicating that HS^- formation led to negative current generation through the PHT mechanism. That is, HS^- on the surface reformed H_2S via reaction $HS^- + H_2S \rightarrow H_2S + HS^-$. Furthermore, this process continued until the negative charge (HS^-) reached the metal substrate. The REMPI laser shots were timed at ~0.7 μs after the PSD laser shots, aligning with the peak of the time-of-flight distribution for HS radicals from the solid surface to probe laser, as shown in Figure 2(c). The time-of-flight distribution for the HS radicals photodesorbed from H_2S solids was reproduced well by the Maxwell–Boltzmann distribution[44], with ~2100 K translational energy. This energy is comparable to that for photodesorbed OH from ice in the previous experiments[36], suggesting the HS photodesorption mechanism similar to the OH case, that is, photoabsorption of OH-$(H_2O)_n$ complex and subsequent desorption. Figure 2(a) and (c) confirmed that the HS intensity decreased upon electron exposure.

ΔI was defined as the increase in the negative current, and Δ[HS] was defined as the decrease in HS density, that is, $([HS]_{OFF} - [HS]_{ON})/[HS]_{OFF}$, where $[HS]_{ON}$ and $[HS]_{OFF}$ represented the detected HS intensities under simultaneous electron and UV exposure and only UV exposure, respectively. A correlation between these parameters is plotted in Figure 2(b). Δ[HS] linearly increased with ΔI, as previously observed in H_2O ice[13], suggesting that negative current transmission was directly promoted by HS radical consumption. The measurement was initiated by gradually increasing the incident electron flux. By using another fresh sample, additional measurement was conducted by decreasing the electron flux in the same incident electron flux range. Because no hysteresis by electron and 193 nm UV exposure could be seen in Figure 2(b), the correlation was independent of the dose of incident electrons and 193 nm UV photons. The fitted line had a small Δ[HS] intercept of ~0.1, which indicated that ~10% of the detected HS radicals could be consumed by electrons on the solid surface without generating a negative

current. Moreover, some HS radicals may have desorbed as anions (HS^-) following electron capture, driven by an exothermicity of 2.3 eV, while experiencing Colomb forces from the negatively charged solid surface. A similar concept is chemical desorption, as explained for the recombination between H and HS[45]. However, most HS radicals, ~90%, may potentially contribute to negative current generation through PHT by forming HS^- in H_2S solids.

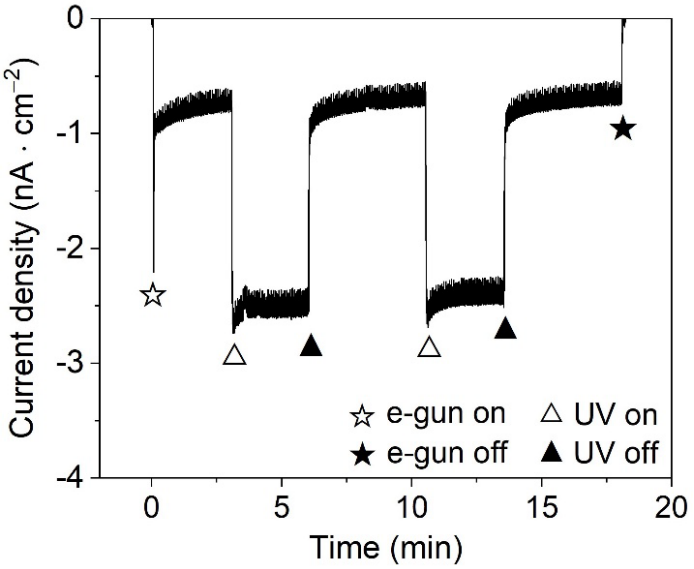

Figure 3. Temporal variation in the negative current during the sequential 193 nm UV irradiation of NH_3 solids at 10 K with continuous electron gun operation. Similar to that for pure H_2S solids, ΔI of ~2 nA cm^{-2} was observed by the co-exposure of UV and electrons. NH_2 radicals photodissociated by UV on the NH_3 solid surface were not detected by the PSD-REMPI method.

The behavior of negative currents in a pure NH_3 solid at 10 K is shown in Figure 3. Similar to that observed for pure H_2S solids, ΔI of ~2 nA cm^{-2} was detected upon co-exposure of UV and electrons at 3 nA cm^{-2} incident current. In this case, NH_2 radicals formed by UV photolysis likely reacted with electrons to form NH_2^- on the NH_3 solid surface, which contributed to the negative currents. Although we measured PSD-REMPI spectra of NH_2 photodesorbed from the

NH_3 solid at 416–417 and 433–434 nm[46], no significant increase in NH_2 signal intensities was confirmed after the UV photolysis of the solids. We attributed this observation to the fact that the NH_2 REMPI signals can significantly originate from the REMPI process of gaseous NH_3. In fact, we found that NH_3 was also photodesorbed from the NH_3 solid surface by the PSD laser. The photodesorbed NH_3 can be dissociated into NH_2 + H by multiphoton process induced by the REMPI laser radiation at 416–417 and 433–434 nm[46], and NH_2 radicals thus generated can be further ionized. We deduce that this process obscured the REMPI intensity variation of NH_2 originating solely from surface NH_2. Thus, we could not establish a correlation between the negative current and variation of surface NH_2. Nevertheless, because NH_2 was the primary product of the 193 nm photolysis of NH_3 with a quantum yield close to unity[47], NH_2 was the most likely candidate for triggering PHT, rather than other radicals such as NH.

The temperature dependence of ΔI for H_2S and NH_3 solids was further investigated at 10–50 K to examine the reaction barrier of PHT for both solids. However, no significant dependence was observed in this temperature range. The same behavior was confirmed for the negative currents transmitted through ice during UV and electron co-exposure at < 50 K, suggesting a barrierless PHT reaction in ice[12]. While a temperature dependence of proton transfer in ice has previously been reported[7,48], our findings suggest an apparent barrierless mechanism for the PHT induced negative charge transport through the H_2S, NH_3, and H_2O solids. It should be noted that H_2S solid was reported to convert from amorphous to crystallin phase at temperatures around 40 – 50 K[49] whereas NH_3 solid is known to be in amorphous phase below 50 K[50]. The possible phase transformation of H_2S would not affect PHT as demonstrated for water ice[13]. For water ice, computational study also suggested that OH^- transmission mechanisms through amorphous and crystalline ice are similar. However, to get further insights, more quantitative investigations on the

effect of the ice structure are desirable[13]. For example, previous quantum chemical calculations searched only the barrierless or low barrier trajectories in ice which enable negative current flow[12]. We do not claim that all pathways in ice are barrierless. As demonstrated in our previous paper[13], the negative current flow through ice decreases with the ice thickness. We interpreted this observation as a part of OH^- is trapped within ice due to the presence of sizable barriers.

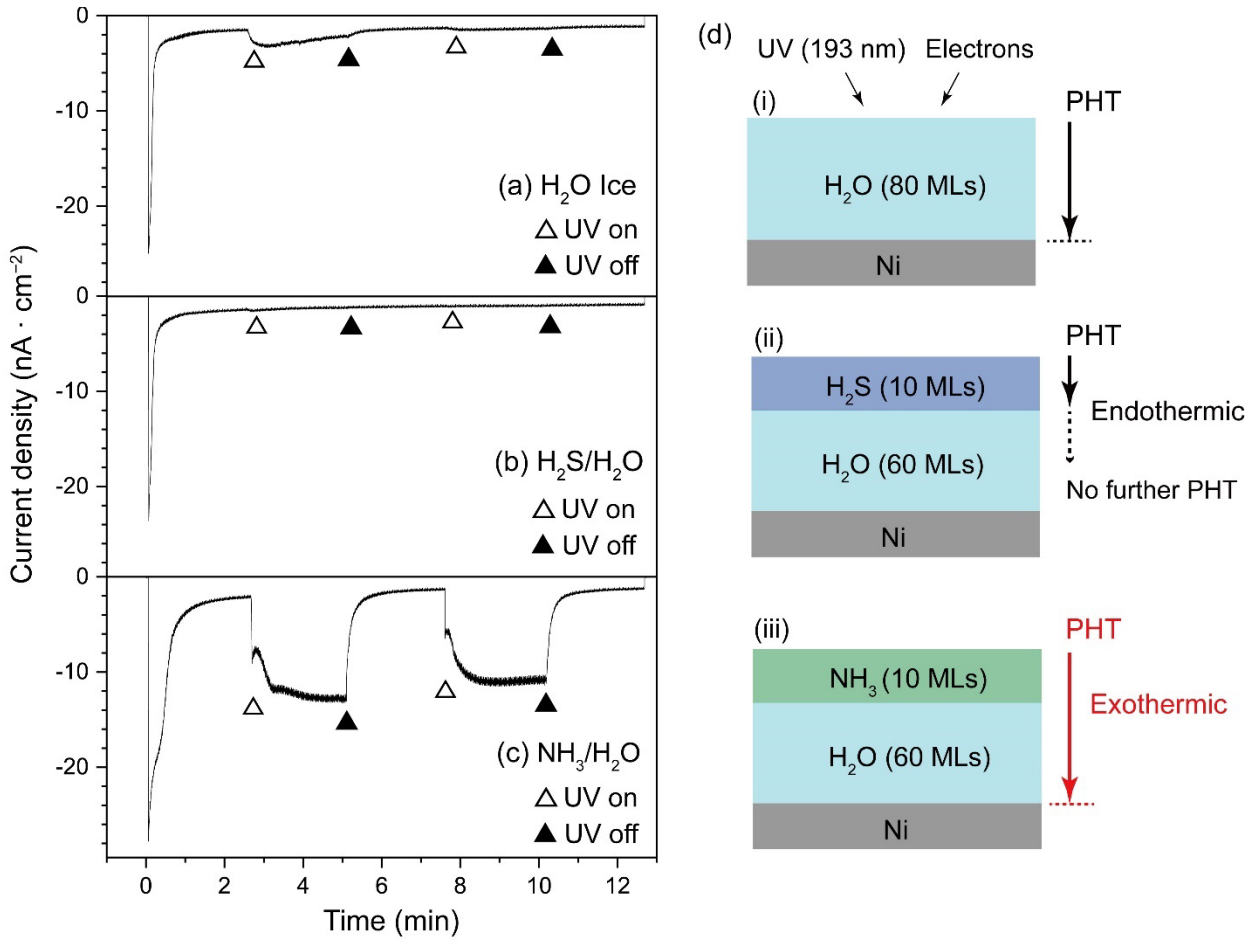

Figure 4. Temporal variation in the negative current during the sequential 193 nm UV irradiation of (a) ice and (b) H_2S/H_2O and (c) NH_3/H_2O bilayer solids at 10 K with continuous electron gun operation. A schematic diagram for each case is illustrated by (i), (ii), and (iii) in (d).

To investigate the effect of exothermicity on PHT at the heterogenous interface, negative currents were measured for H_2S/H_2O and NH_3/H_2O solids at 10 K. As mentioned earlier, for

H_2S/H_2O and NH_3/H_2O bilayer solids, the negative charge delivery behavior depends on the exothermicity of PHT at the interface between ice and the upper layer of molecules. During the measurement, the incident electron currents were controlled at ~30 nA cm^{-2}, and comparable ΔI was expected to be transmitted through the bilayer solids.

We first confirmed that 193 nm UV irradiation ineffectively induced PHT in ice. The temporal variation of negative currents measured for ice exposed to 193 nm UV photons and electrons at 10 K are shown in Figure 4(a). A sharp transient peak was observed for ice during electron exposure, and the negative currents did not significantly increase, even after 193 nm UV irradiation. Because the photoabsorption cross section of ice was negligible ($<10^{-20}$ cm^2) at 193 nm[51], OH radicals were inefficiently produced by photolysis. Nevertheless, the photoabsorption of surface H_2O close to the dimer structure $(H_2O)_2$ could have still occurred[52], which may have contributed to OH formation on ice surface. Thus, a small current increase was observed upon 193 nm UV irradiation.

In the layered H_2S/H_2O solid, nearly no negative currents were observed during 193 nm UV irradiation, as shown in Figure 4(b). First, H_2S deposition on ice may have obscured the water dimer structure, hindering surface H_2O photodissociation. Therefore, negative currents would require reaction $HS^- + H_2O \rightarrow H_2S + OH^-$. However, this reaction is endothermic because the proton affinity of HS^- (15.0 eV) is lower than that of OH^- (17.0 eV); thus, HS^- is less likely to cause proton abstraction from H_2O[30].

In contrast, with the deposition of NH_3 layers on ice, the negative currents significantly increased, as shown in Figure 4(c). The process is explained by the following exothermic reaction: $NH_2^- + H_2O \rightarrow NH_3 + OH^-$. Because NH_2^- has a proton affinity of 17.5 eV, which is

higher than that of OH^- (17.0 eV)[30], proton abstraction by NH_2^- from H_2O should occur at the NH_3/H_2O solid interface.

Previous quantum chemical calculations revealed that the total energy of ice decreased as OH^- moved from the surface toward the nickel substrate[12,13]. This finding aligned with our experimental observation of negative currents in ice, even at 10 K. Although the detailed mechanisms of PHT in the H_2S and NH_3 solid have not been rationalized by calculations, the difference in the negative current behaviors between NH_3/H_2O and H_2S/H_2O solids can be explained in terms of the proton affinities of HS^-, NH_2^- and OH^- [30]; that is, exothermic and endothermic proton abstraction reactions at the bilayer interfaces, as described above.

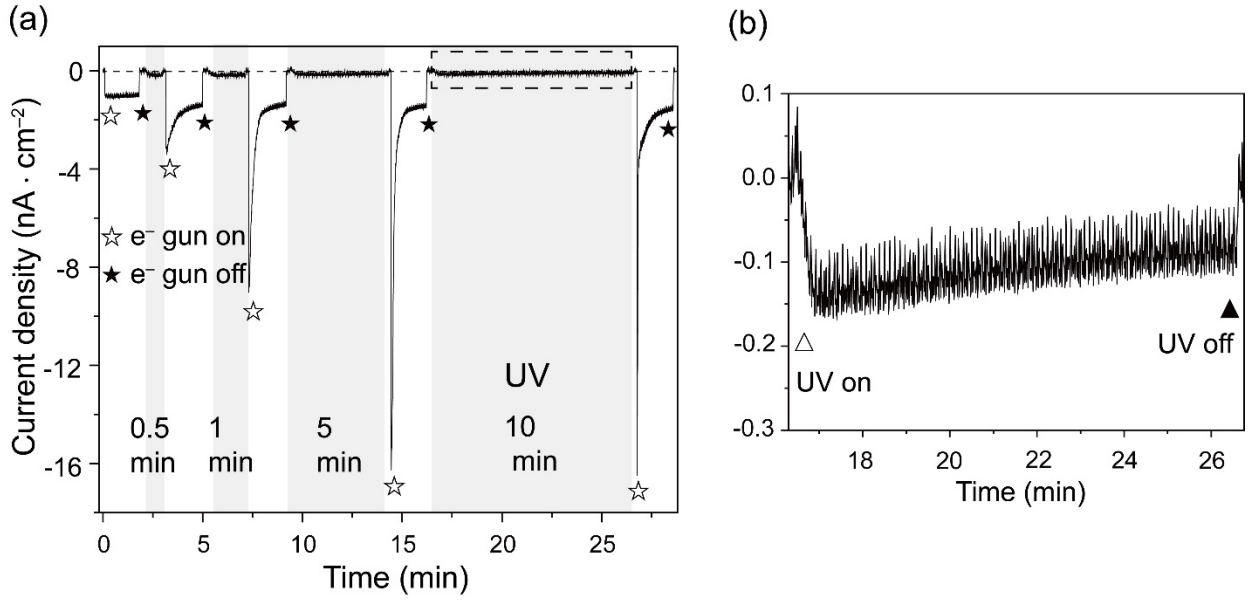

Figure 5. (a) Negative currents upon the sequential exposure of NH_3/H_2O bilayer solids to electrons and 193 nm UV photons. The 193 nm UV irradiation durations were 0.5, 1, 5, and 10 min. (b) Enlarged view for 10 min UV irradiation in the dashed square in Figure 4(a). A five-point moving average was used to obtain the smoothed line of the data plots.

An additional experiment was conducted to elucidate the relationship between the abundance of surface NH_2 and negative current generated through the NH_3/H_2O bilayer solid. The experimental procedure consists of three steps. First, the electron gun was operated for 20 min to supply electrons to the NH_3/H_2O surface. Next, after a specified UV irradiation duration, the solid was exposed to electrons for ~1 min. Then, this process was repeated four times with UV irradiation durations of 0.5, 1, 5, and 10 min. The corresponding UV fluence was varied from 3×10^{16} to 6×10^{17} photons cm^{-2}. Negative currents with different NH_2 abundances on the surface were monitored by controlling the 193 nm UV irradiation duration. A similar experiment was conducted for ice at 10 K[12], suggesting that surface OH accumulation led to the larger peak current upon electron irradiation.

Figure 5(a) shows the temporal variation of negative currents through the NH_3/H_2O solid during the sequential exposure to electrons and UV. The first appearance of a negative current before initializing UV exposure corresponded to the bias current (~1 nA cm^{-2}) without UV exposure in Figure 4(c). This current was not caused by the PHT mechanism. The peak current at the onset of electron impinging increased with the UV irradiation duration preceding it. The identical experiment was also conducted for a H_2S/H_2O solid, but the negative current by PHT could not be induced and the peak current at the electron impinging remained very low ($\leq$ 2.5 nA cm^{-2}) irrespective of the UV irradiation duration. The contrasting results indicated that the current enhancement for the NH_3/H_2O solid was caused by PHT through surface NH_2 accumulation by UV irradiation. Over a UV exposure time of 5 min (fluence: 3×10^{17} photons cm^{-2}) in Figure 5(a), the peak current upon electron irradiation was nearly saturated, which suggested that NH_2 accumulation became saturated over a fluence on the order of 10^{17} photons cm^{-2}. A previous infrared spectroscopy study[31] also reported that the number density of NH_2 in UV-irradiated NH_3

solids was steady over a fluence on the order of 10^{17} photons cm^{-2}. In addition, Figure 5(b) shows an enlarged view of the negative currents during 10 min UV irradiation in Figure 5(a). The flow of a weak current (~0.15 nA cm^{-2}) is clearly visible during UV irradiation, even without the supply of electrons. Such negative currents during UV irradiation were not observed for H_2S/H_2O solids. These results confirm that the electrons accumulated in solids attached to NH_2 generated by UV irradiation preceding the sequence of electron injections, resulting in the weak current due to PHT. In our previous study with ice, UV irradiation in the Lyman-α region caused photoelectron emission from the nickel substrate, leading to low positive currents[12]. This study applied 193 nm UV irradiation with a photon energy of 6.4 eV. Although the work function of nickel (and nickel oxide) substrate is approximately 5.2-5.6 eV[53], efficient photoemission is known to require additional energies of 1 eV and more[54, 55]. That is, the present photon energy was not high enough for efficient photoemission. In fact, photocurrent was not observed when the bare nickel substrate without ice was exposed to photons at 193 nm.

In summary, we investigated the PHT mechanism in hydrogen-bonded solids of H_2S and NH_3, as well as in bilayer solids of H_2S/H_2O and NH_3/H_2O, at 10 K. The negative current behavior observed through H_2S or NH_3 solids upon simultaneous exposure to 193 nm photons and electrons indicated the occurrence of PHT in solids. The variation in HS densities was explained by a scenario where surface HS radicals were produced by UV photolysis and subsequently captured electrons on the H_2S solid surface. The PHT mechanism was possibly triggered by HS^- and NH_2^- species generated through photolysis and electron capture. The incident electron currents supplied to the surface determined the current caused by PHT (i.e., ΔI) through H_2S solids. To further explore the PHT mechanism in solids, we conducted experiments using bilayer solids. An increase in the negative current was observed exclusively for the NH_3/H_2O solid.

Because reaction $NH_2^- + H_2O \rightarrow NH_3 + OH^-$ is exothermic, proton abstraction by NH_2^- from lower H_2O molecules could occur at the bilayer interface. Then, a sequence of PHT by OH^- in ice reached the metal substrate and was detected as the negative current. Our findings suggested that PHT could be a universal electrochemical property of hydrogen-bonded solids at very low temperatures. Other solids should be examined in future to further clarify PHT mechanisms and investigate the relationship between PHT efficiency and hydrogen bond strength.

ASSOCIATED CONTENT

Supporting Information.

A detailed description of the experimental methodology

Corresponding author

Naoki Watanabe

Institute of Low Temperature Science, Hokkaido University; *Kita-19, Nishi-8, Kita-ku, Sapporo, 060-0819, Japan*; ORCID: 0000-0001-8408-2872; Email: watanabe@lowtem.hokudai.ac.jp

Notes

Authors declare no competing financial interest.

ACKNOWLEDGMENT

We thank the technical staff of ILTS for improving our apparatus. This study was partly supported by JSPS Grant-in-Aids for Specially Promoted Research (JP17H06087) and Early-

Career Scientists (JP20K14534); a grant for the Joint Research Program of the Institute of Low Temperature Science, Hokkaido University (21G012 and 22K002); and the Kurita Water and Environment Foundation (23D005).

REFERENCES

(1) Marx, D. Proton Transfer 200 Years after von Grotthuss: Insights from Ab Initio Simulations. *ChemPhysChem* **2006**, *7* (9), 1848–1870.

(2) Bountis, T. *Proton Transfer in Hydrogen-Bonded Systems*; Springer Science & Business Media, 2012.

(3) Khistyaev, K.; Golan, A.; Bravaya, K. B.; Orms, N.; Krylov, A. I.; Ahmed, M. Proton Transfer in Nucleobases Is Mediated by Water. *J. Phys. Chem. A* **2013**, *117* (31), 6789–6797.

(4) Demchenko, A. P. Proton Transfer Reactions: From Photochemistry to Biochemistry and Bioenergetics. *BBA Adv.* **2023**, *3*, 100085.

(5) Abel, B. Hydrated Interfacial Ions and Electrons. *Annu. Rev. Phys. Chem.* **2013**, *64*, 533–552.

(6) Agmon, N. The Grotthuss Mechanism. *Chem. Phys. Lett.* **1995**, *244* (5), 456–462.

(7) Uritski, A.; Presiado, I.; Erez, Y.; Gepshtein, R.; Huppert, D. Temperature Dependence of Proton Diffusion in I_h Ice. *J. Phys. Chem. C* **2009**, *113* (23), 10285–10296.

(8) Tahat, A.; Martí, J. Dynamical Aspects of Intermolecular Proton Transfer in Liquid Water and Low-Density Amorphous Ices. *Phys. Rev. E* **2014**, *89* (5), 052130.

(9) Ghesquière, P.; Mineva, T.; Talbi, D.; Theulé, P.; Noble, J. A.; Chiavassa, T. Diffusion of Molecules in the Bulk of a Low Density Amorphous Ice from Molecular Dynamics Simulations. *Phys. Chem. Chem. Phys.* **2015**, *17* (17), 11455–11468.

(10) Aoki, M.; Hara, N.; Ikeda-Fukazawa, T. Surface Diffusion of Proton in Amorphous Ice. *Surf. Sci.* **2019**, *684*, 58–61.

(11) Presiado, I.; Lal, J.; Mamontov, E.; Kolesnikov, A. I.; Huppert, D. Fast Proton Hopping Detection in Ice I_h by Quasi-Elastic Neutron Scattering. *J. Phys. Chem. C* **2011**, *115* (20), 10245–10251.

(12) Watanabe, N.; Sameera, W. M. C.; Hidaka, H.; Miyazaki, A.; Kouchi, A. Ultraviolet-Photon Exposure Stimulates Negative Current Conductivity in Amorphous Ice below 50 K. *Chem. Phys. Lett.* **2019**, *737*, 136820.

(13) Kitajima, K.; Nakai, Y.; Sameera, W. M. C.; Tsuge, M.; Miyazaki, A.; Hidaka, H.; Kouchi, A.; Watanabe, N. Delivery of Electrons by Proton-Hole Transfer in Ice at 10 K: Role of Surface OH Radicals. *J. Phys. Chem. Lett.* **2021**, *12* (1), 704–710.

(14) Collier, W. B.; Ritzhaupt, G.; Devlin, J. P. Spectroscopically Evaluated Rates and Energies for Proton Transfer and Bjerrum Defect Migration in Cubic Ice. *J. Phys. Chem.* **1984**, *88* (3), 363–368.

(15) Cowin, J. P.; Tsekouras, A. A.; Iedema, M. J.; Wu, K.; Ellison, G. B. Immobility of Protons in Ice from 30 to 190 K. *Nature* **1999**, *398* (6726), 405.

(16) Steiner, T. The Hydrogen Bond in the Solid State. *Angew. Chem. Int. Ed.* **2002**, *41* (1), 49–76.

(17) Fitch, A. N.; Cockcroft, J. K. A New Structure for the Lowest-Temperature Phase of Solid Hydrogen Sulphide. *J. Chem. Soc. Chem. Commun.* **1990**, *0* (6), 515–516.

(18) Hewat, A. W.; Riekel, C. The Crystal Structure of Deuteroammonia between 2 and 180 K by Neutron Powder Profile Refinement. *Acta Crystallogr. A* **1979**, *35* (4), 569–571.

(19) Fathe, K.; Holt, J. S.; Oxley, S. P.; Pursell, C. J. Infrared Spectroscopy of Solid Hydrogen Sulfide and Deuterium Sulfide. *J. Phys. Chem. A*. **2006**, 110, 10793–10798.

(20) Holt, J. S.; Sadoskas, D.; Pursell, C. J. Infrared Spectroscopy of the Solid Phases of Ammonia. *J. Chem. Phys.* **2004**, *120* (15), 7153–7157.

(21) Zheng, W.; Kaiser, R. I. An Infrared Spectroscopy Study of the Phase Transition in Solid Ammonia. *Chem. Phys. Lett.* **2007**, *440* (4), 229–234.

(22) Tomoda, S. Ionization of the Ammonia Dimer: Proton Transfer in the Ionic State. *Chem. Phys.* **1986**, *110* (2), 431–445.

(23) Gilli, G.; Gilli, P. Towards an Unified Hydrogen-Bond Theory. *J. Mol. Struct.* **2000**, *552* (1), 1–15.

(24) Barroso, M.; Arnaut, L. G.; Formosinho, S. J. Absolute Rate Calculations: Atom and Proton Transfers in Hydrogen-Bonded Systems. *ChemPhysChem* **2005**, *6* (2), 363–371.

(25) Do, H.; Besley, N. A. Proton Transfer or Hemibonding? The Structure and Stability of Radical Cation Clusters. *Phys. Chem. Chem. Phys.* **2013**, *15* (38), 16214–16219.

(26) Wang, D.; Fujii, A. Spectroscopic Observation of Two-Center Three-Electron Bonded (Hemi-Bonded) Structures of $(H_2S)_n^+$ Clusters in the Gas Phase. *Chem. Sci.* **2017**, *8* (4), 2667–2670.

(27) Stiles, D. A.; Tyerman, W. J. R.; Strausz, O. P.; Gunning, H. E. Photolysis of Group vi Hydrides: I. Solid H_2S, H_2S_2, and D_2S. *Can. J. Chem.* **1966**, *44* (18), 2149–2155.

(28) Cazaux, S.; Carrascosa, H.; Muñoz Caro, G. M.; Caselli, P.; Fuente, A.; Navarro-Almaida, D.; Riviére-Marichalar, P. Photoprocessing of H_2S on Dust Grains: Building S Chains in Translucent Clouds and Comets. *Astron. Astrophys.* **2022**, *657*, A100.

(29) Heays, A. N.; Bosman, A. D.; van Dishoeck, E. F. Photodissociation and Photoionisation of Atoms and Molecules of Astrophysical Interest. *Astron. Astrophys.* **2017**, 602, A105.

(30) NIST Chemistry WebBook, NIST Standard Reference Database Number 69.

(31) Gerakines, P. A.; Schutte, W. A.; Ehrenfreund, P. Ultraviolet Processing of Interstellar Ice Analogs. I. Pure Ices. *Astron, Astrophys.* **1996**, *312*, 289–305.

(32) Loeffler, M. J.; Baragiola, R. A. Photolysis of Solid NH_3 and NH_3-H_2O Mixtures at 193 nm. *J. Chem. Phys.* **2010**, *133* (21), 214506.

(33) Martín-Doménech, R.; Cruz-Díaz, G. A.; Muñoz Caro, G. M. UV Photoprocessing of NH_3 Ice: Photon-Induced Desorption Mechanisms. *Mon. Not. R. Astron. Soc.* **2017**, *473* (2), 2575–2582.

(34) Watanabe, N.; Kimura, Y.; Kouchi, A.; Chigai, T.; Hama, T.; Pirronello, V. Direct Measurements of Hydrogen Atom Diffusion and the Spin Temperature of Nascent H_2 Molecule on Amorphous Solid Water. *Astrophys. J. Lett.* **2010**, *714*, :L233-L237.

(35) Tsuge, M.; Molpeceres, G.; Aikawa, Y.; Watanabe, N. Surface Diffusion of Carbon Atoms as a Driver of Interstellar Organic Chemistry. *Nat. Astron.* **2023**, *7* (11), 1351–1358.

(36) Miyazaki, A.; Watanabe, N.; Sameera, W. M. C.; Nakai, Y.; Tsuge, M.; Hama, T.; Hidaka, H.; Kouchi, A. Photostimulated Desorption of OH Radicals from Amorphous Solid Water: Evidence for Interaction of Visible Light with OH-Ice Complex. *Phys. Rev. A* **2020**, 102, 052822.

(37) Miyazaki, A.; Tsuge, M.; Hidaka, H.; Nakai, Y.; Watanabe, N. Direct Determination of the Activation Energy for Diffusion of OH Radicals on Water Ice. *Astrophy, J. Lett.* **2022**, *940* (1), L2.

(38) Western, C. M. PGOPHER: A Program for Simulating Rotational, Vibrational and Electronic Spectra. *J. Quant. Spectrosc. Radiat. Transf.* **2017**, *186*, 221–242.

(39) Milan, J. B.; Buma, W. J.; de Lange, C. A. Two-Photon Resonance Enhanced Multiphoton Ionization Photoelectron Spectroscopy of the SH (SD) Radical below and above the Lowest Ionization Threshold. *J. Chem. Phys.* **1996**, *105* (16), 6688–6712.

(40) Sagi, R.; Akerman, M.; Ramakrishnan, S.; Asscher, M. Solid Ammonia Charging by Low-Energy Electrons. *J. Phys. Chem. C* **2021**, *125* (7), 3845–3858.

(41) Horowitz, Y.; Asscher, M. Low Energy Charged Particles Interacting with Amorphous Solid Water Layers. *J. Chem. Phys.* **2012**, *136*, 134701.

(42) Szmytkowski, C.; Maciąg, K. Absolute Total Electron-Scattering Cross Section of H_2S. *Chem. Phys. Lett.* **1986**, *129* (3), 321–324.

(43) Brotton, S. J.; Vyskocil, E.; Kedzierski, W.; McConkey, J. W. Dissociative Excitation of H_2S by Electron Impact. *Phys. Rev. A* **2009**, *79* (4), 042709.

(44) Zimmermann, F. M.; Ho, W. Velocity Distributions of Photochemically Desorbed Molecules. *J. Chem. Phys.* **1994**, *100*, 7700.

(45) Oba, Y.; Tomaru, T.; Lamberts, T.; Kouchi, A.; Watanabe, N. An Infrared Measurement of Chemical Desorption from Interstellar Ice Analogues. *Nat. Astron.* **2018**, *2*, 228–232.

(46) Glownia, J. H.; Riley, S. J.; Colson, S. D.; Nieman, G. C. The MPI Spectrum of Expansion-cooled Ammonia: Photophysics and New Assignments of Electronic Excited States. *J. Chem. Phys.* **1980**, *73* (9), 4296‑4309.

(47) Donnelly, V. M.; Baronavski, A. P.; McDonald, J. R. ArF Laser Photodissociation of NH_3 at 193 nm: Internal Energy Distributions in NH_2 $\tilde{X}^2B_1$ and $\tilde{A}^2A_1$, and Two-Photon Generatin of NH A $^3\Pi$ and b $^1\Sigma^+$. *Chem. Phys.* **1979**, *43* (2), 271–281.

(48) Lee, D. H.; Kang, H.; Kang, H. Tunneling Diffusion of Excess Protons in Amorphous Solid Water at 10 and 80 K. *J. Phys. Chem. C* **2019**, *123* (6), 3657–3663.

(49) Fathe, K.; Holt, J. S.; Oxley, S. P.; Pursell, C. J. Infrared Spectroscopy of Solid Hydrogen Sulfide and Deuterium Sulfide. *J. Phys. Chem. A*. **2006**, 110, 10793–10798.

(50) Dawes, A.; Mukerji, R. J.; Davis, M. P.; Holtom, P. D.; Webb, S. M.; Sivaraman, B.; Hoffmann, S. V.; Shaw, D. A.; Mason, N. J. Morphological Study into the Temperature Dependence of Solid Ammonia under Astrochemical Conditions Using Vacuum Ultraviolet and Fourier-Transform Infrared Spectroscopy. *J. Chem. Phys.* **2007**, *126* (24), 244711.

(51) Yabushita, A.; Hashikawa, Y.; Ikeda, A.; Kawasaki, M.; Tachikawa, H. Hydrogen Atom Formation from the Photodissociation of Water Ice at 193 nm. *J. Chem. Phys.* **2004**, 120, 5463.

(52) Harvey, J. N.; Jung, J. O.; Gerber, R. B. Ultraviolet Spectroscopy of Water Clusters: Excited Electronic States and Absorption Line Shapes of $(H_2O)_n$, n=2–6. *J. Chem. Phys.* **1998**, *109* (20), 8747–8750.

(53) Anderson, J. S.; Klemperer, D. F. Photoelectric Measurements on Nickel and Nickel Oxide Film. *Proc. R. Soc. Lond.* **1960**, *258* (1294), 350–376.

(54) Guillot, C.; Ballu, Y.; Paigné, J.; Lecante, J.; Jain, K. P.; Thiry, P.; Pinchaux, R.; Pétroff, Y.; Falicov, L. M. Resonant Photoemission in Nickel Metal. *Phys. Rev. Lett.* **1977**, *39* (25), 1632–1635.

(55) Barth, J.; Kalkoffen, G.; Kunz, C. Resonance Enhancement of the Nickel d-Band Photoemission. *Phys. Lett. A* **1979**, *74* (5), 360–362.